Supporting Information

Interface Engineering of 2D-C_3N_4/NiFe-LDH Heterostructure for Highly Efficient Photocatalytic Hydrogen Evolution

*Jia Yan,[1,†] Xiandi Zhang,[1,†] Weiran Zheng,[1] and Lawrence Yoon Suk Lee[1,2,]**

[1] Department of Applied Biology and Chemical Technology and State Key Laboratory of Chemical Biology and Drug Discovery, The Hong Kong Polytechnic University, Hung Hom, Kowloon, Hong Kong SAR, China.

[2] Research Institute for Smart Energy, The Hong Kong Polytechnic University, Hung Hom, Kowloon, Hong Kong SAR, China.

* E-mail: lawrence.ys.lee@polyu.edu.hk (L. Y. S. Lee)

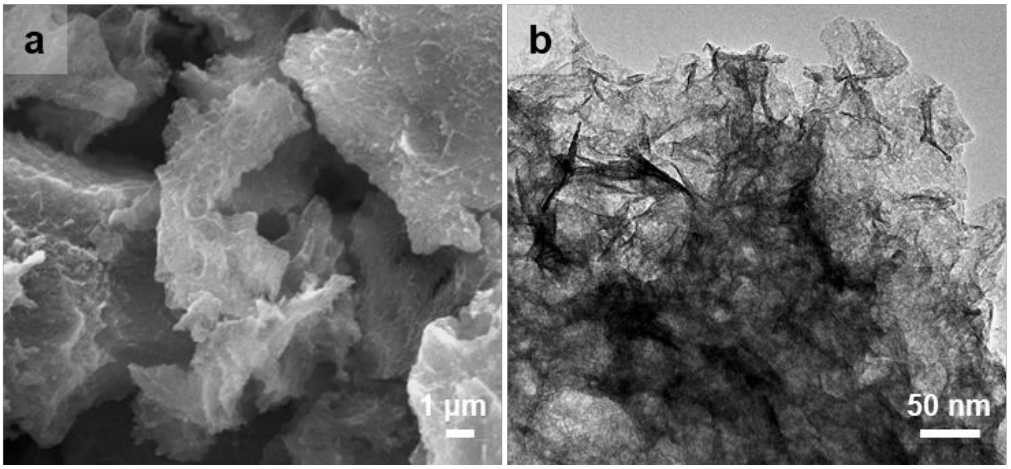

Figure S1. (a) SEM and (b) TEM images of LDH-3 sample with NH_4F added at the last step of synthesis.

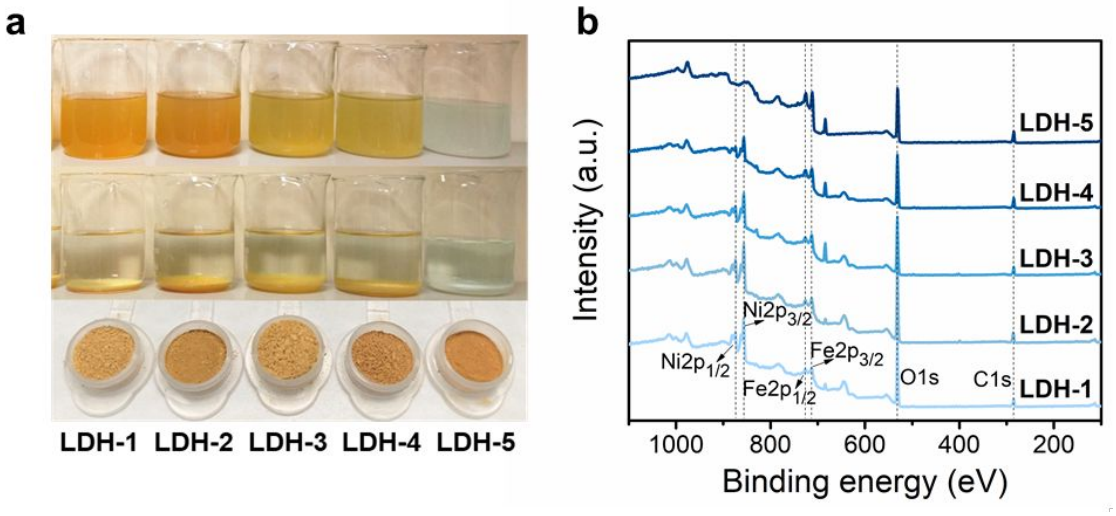

Figure S2. (a) Digital photos showing the color change of LDH samples during the synthesis (Top: after 5 h; Middle: after 24 h; Bottom: final samples). (b) Survey XPS spectra of LDH samples.

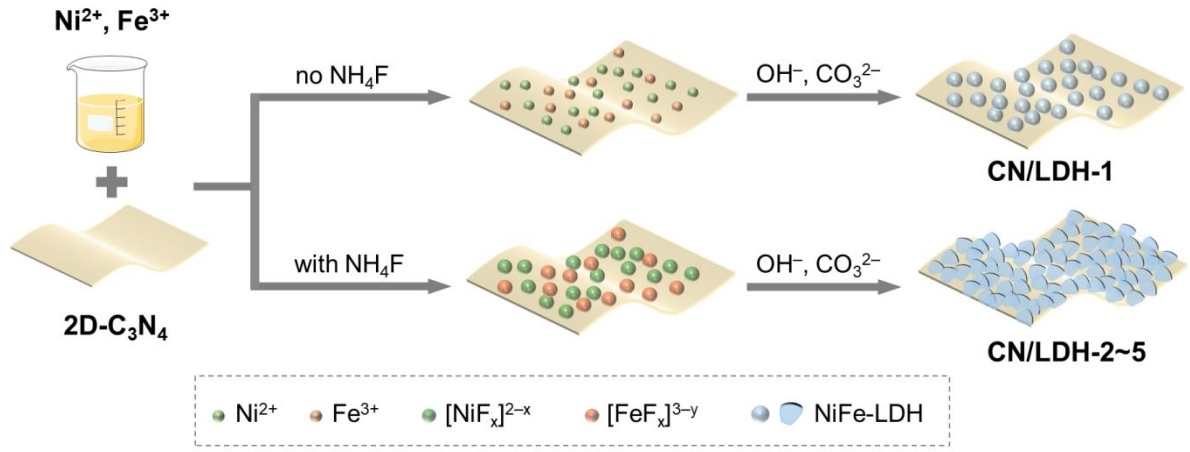

Figure S3. An overview of the synthetic procedure for 2D-C_3N_4/NiFe-LDH heterostructure.

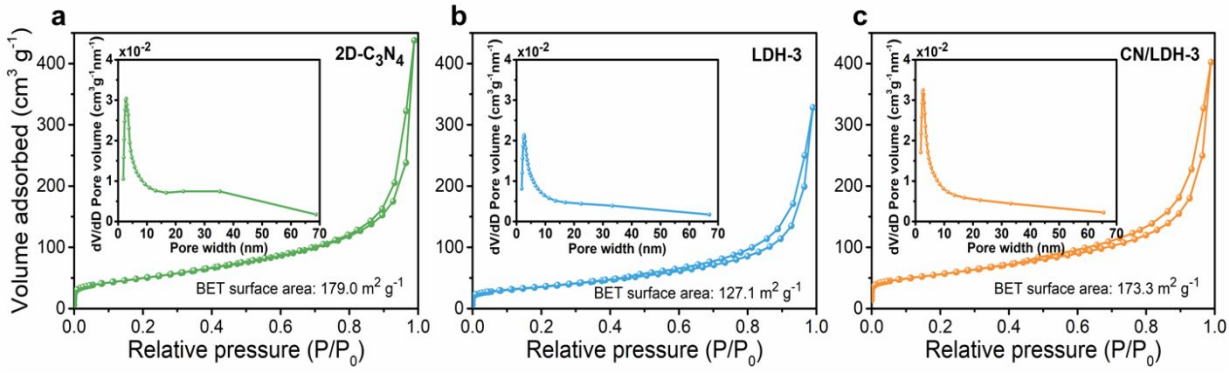

Figure S4. N_2 adsorption–desorption isotherms of (a) 2D-C_3N_4, (b) LDH-3, and (c) CN/LDH-3. Insets are the corresponding pore size distribution curves.

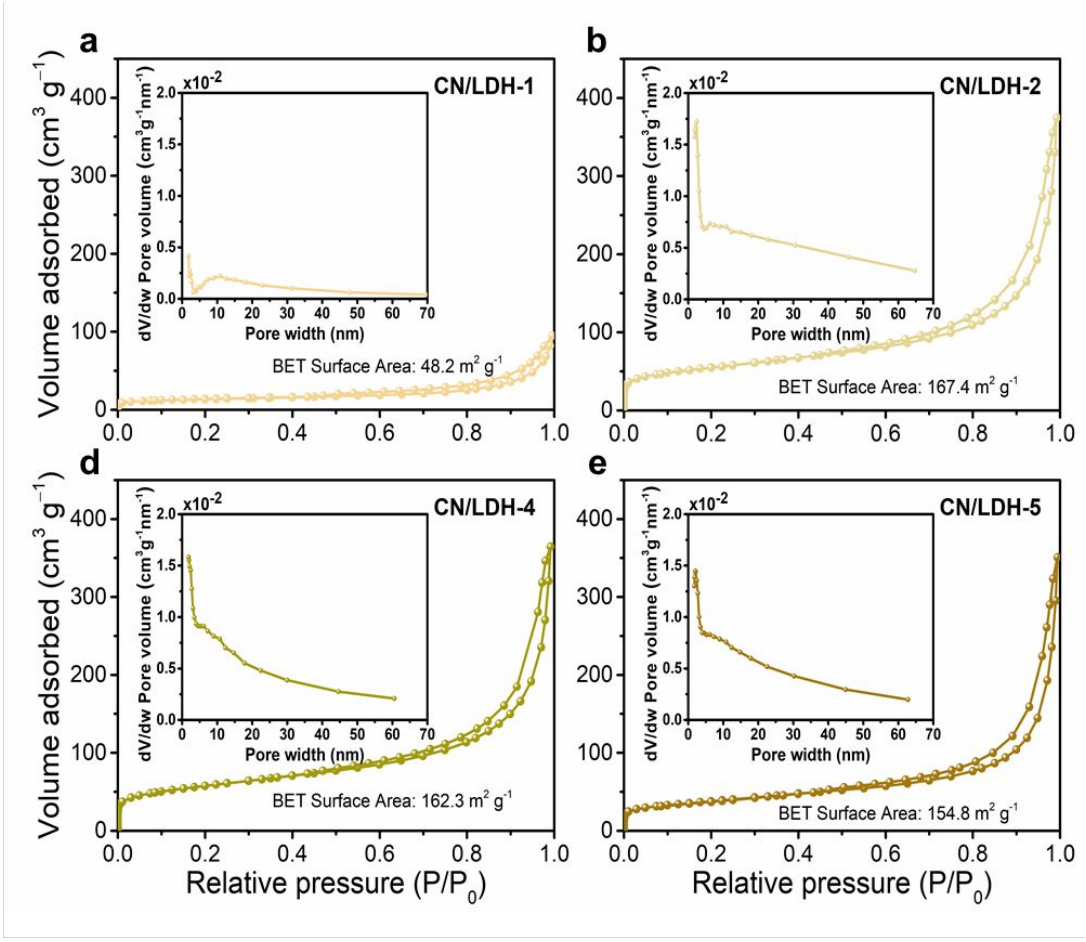

Figure S5. N_2 adsorption–desorption isotherms of (a) CN/LDH-1, (b) CN/LDH-2, (c) CN/LDH-4, and (d) CN/LDH-5. Insets are the corresponding pore size distribution curves.

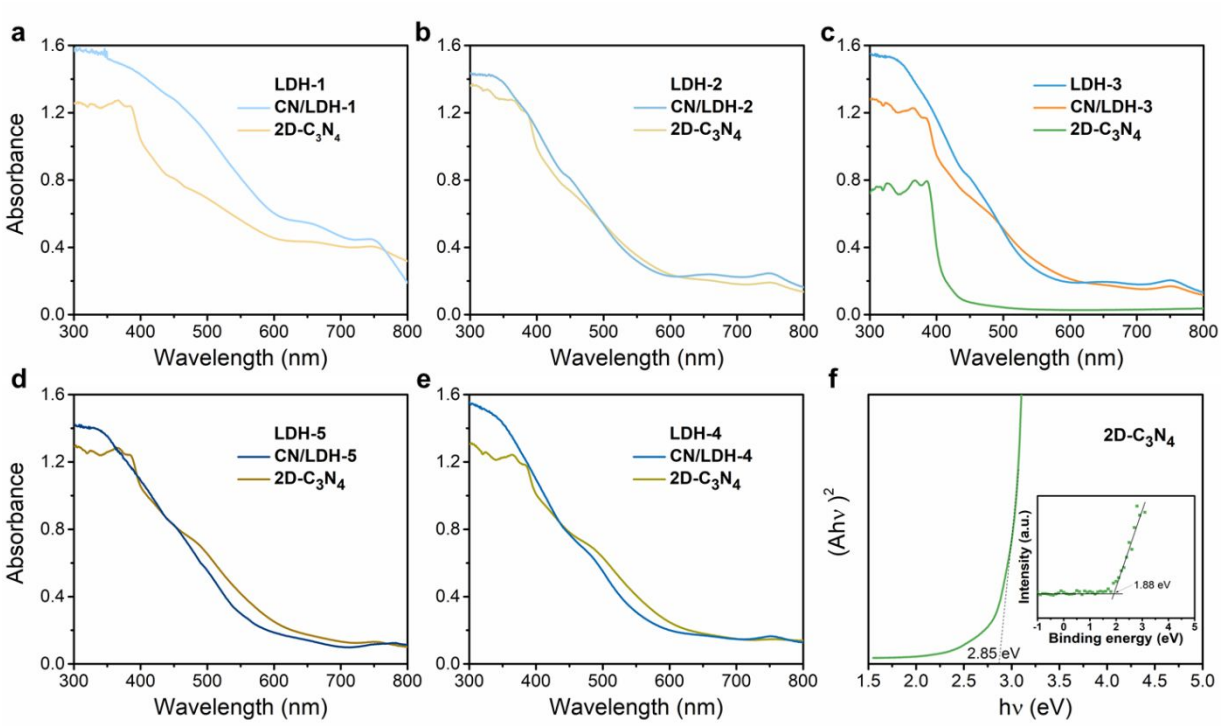

Figure S6. (a–e) UV–vis spectra of LDH, CN/LDH samples, and 2D-C_3N_4. (f) Estimated band gap of 2D-C_3N_4. Inset shows the VB_{XPS} of 2D-C_3N_4.

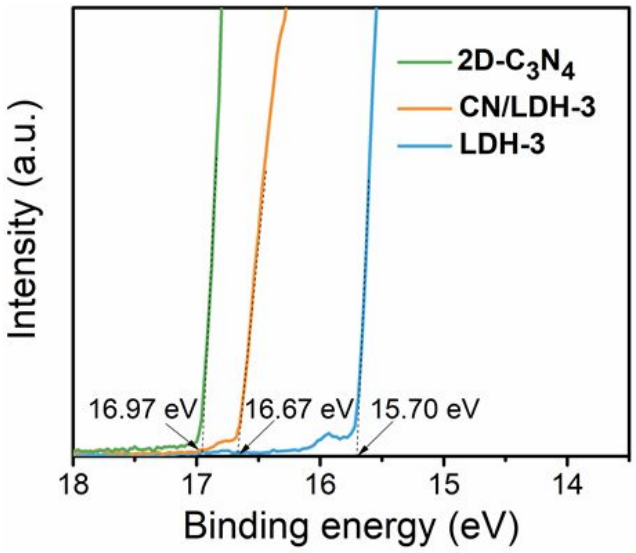

Figure S7. UPS spectra of 2D-C_3N_4, LDH-3, and CN/LDH-3.

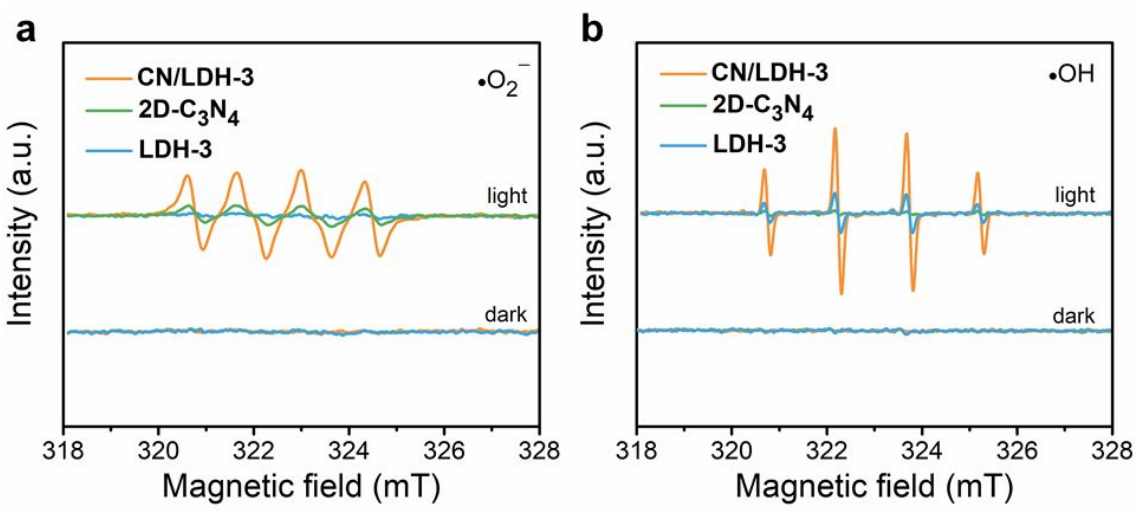

Figure S8. ESR spectra of (a) DMPO-•O_2^- in methanol and (b) DMPO-•OH in aqueous dispersion in the presence of 2D-C_3N_4, LDH-3, and CN/LDH-3.

Apparent quantum efficiency (AQE) was calculated as follows:

$$AQE = \frac{number\ of\ reacted\ electrons}{number\ of\ incident\ photons} \times 100\%$$

$$= \frac{2 \times n \times N_A}{\frac{E \times A \times t}{\hbar \times \frac{c}{\lambda}}} \times 100\%$$

where n is the amount of H_2 molecules generated (3.15×10^{-6} mol), N_A is Avogadro's constant (6.02×10^{23} mol^{-1}), E is average light intensity (1.4 W cm^{-2}), A is irradiation area (4.52 cm^{-2}), t is the irradiation time (3600 s), $\hbar$ is Planck constant (6.626×10^{-34} J·s), c is the speed of light (3×10^8 m s^{-1}), and λ is the wavelength of the monochromatic light (385×10^{-9} m). Using this equation, the AQE of CN/LDH-3 at 385 nm irradiation was estimated as 8.6%.

Table S1. pH values in each synthesis step of LDH samples.

Conditions	pH				
	LDH-1	LDH-2	LDH-3	LDH-4	LDH-5
100 mL solution A (containing $Ni(NO_3)_2$, $Fe(NO_3)_3$, and different amount of NH_4F)	2.1	5.8	5.9	6.0	6.1
60 mL solution B (containing NaOH and Na_2CO_3)	12.5	12.5	12.5	12.5	12.5
After adding 30 mL solution B into solution A	8.4	7.2	7.2	7.1	7.0
After adding 60 mL solution B into solution A	10.6	7.8	7.7	7.6	7.5

Table S2. Ni/Fe ratios in LDH samples based on EDS and ICP-OES analyses.

Method	LDH-1	LDH-2	LDH-3	LDH-4	LDH-5
EDS	2.16	0.97	0.96	0.51	0
ICP-OES	1.91	1.03	0.75	0.27	0

Table S3. Zeta potential of 2D-C_3N_4.

Trial	Zeta Potential (mV)
1	−24.94
2	−25.85
3	−25.15
Average	**−25.31**

Table S4. Fitted resistance parameters for the EIS measurements of 2D-C_3N_4, LDH-3, and CN/LDH-3.

Sample	R_s (Ω)	R_{ct} (Ω)
2D-C_3N_4	59.52	126.4
LDH-3	65.66	81.93
CN/LDH-3	45.29	26.76

Table S5. Lifetimes of photogenerated charge carriers in 2D-C_3N_4, LDH-3, and CN/LDH-3.

Sample	A_1	τ_1 (ns)	A_2	τ_2 (ns)
2D-C_3N_4	0.29	3.00	0.03	17.66
CN/LDH-3	0.26	3.60	0.03	21.14

Table S6. Comparison of recent LDH-based photocatalysts for photocatalytic H_2 evolution.

Photocatalyst	Light source	Reaction conditions	HER rate (mmol g^{-1} h^{-1})	Ref.
NH_2-MIL-125(Ti)/ZnCr-LDH	300 W Xe lamp, $\lambda > 420$ nm	TEOA (0.01 M)	0.128	1
NiFe LDH/N-rGO/g-C_3N_4	125 W Hg lamp, $\lambda \geq 400$ nm	CH_3OH (10 vol.%)	1.254	2
WO_{3-X}/ZnCr LDH	150 W Xe lamp, $\lambda \geq 420$ nm	CH_3OH (10 vol.%)	1.002	3
NiCo-LDH/P-CdS	300 W Xe lamp, $\lambda \geq 400$ nm	lactic acid (10 vol.%)	8.665	4
CdS/ZnCr-LDH	300 W Xe lamp	Na_2S (0.1 M), Na_2SO_3 (0.1 M)	2.164	5
MgAl-LDH/NiS	300 W Xe lamp, $\lambda \geq 420$ nm	CH_3OH (20 vol.%)	0.895	6
g-C_3N_4/NiFe-LDH	125 W Hg lamp, $\lambda \geq 420$ nm	CH_3OH (10 vol.%)	0.774	7
CdS/NiFe LDH	300 W Xe lamp	CH_3OH (10 vol.%)	0.469	8
CdS/CdAl-LDH	300 W Xe lamp, $\lambda \geq 400$ nm	sodium lactate	0.362	9
rGO/$La_2Ti_2O_7$/NiFe-LDH	AM 1.5 illumination	TEOA (10 vol.%)	0.532	10
CdZnS/ZnCr-LDH	300 W Xe lamp, $\lambda \geq 400$ nm	CH_3OH (20 vol.%)	0.916	11
C_3N_4/NiFe-LDH	**450 W solar simulator with an AM 1.5G filter**	**TEOA (10 vol.%)**	**3.087**	**This work**
Pt/C_3N_4/NiFe-LDH			**6.817**	**This work**

References

1 Sohail, M.; Kim, H.; Kim, T. W., Enhanced Photocatalytic Performance of a Ti-Based Metal-Organic Framework for Hydrogen Production: Hybridization with ZnCr-LDH Nanosheets. *Sci. Rep.* **2019**, *9*, 7584.

2 Nayak, S.; Parida, K. M., Deciphering Z-Scheme Charge Transfer Dynamics in Heterostructure NiFe-LDH/N-rGO/g-C_3N_4 Nanocomposite for Photocatalytic Pollutant Removal and Water Splitting Reactions. *Sci. Rep.* **2019**, *9*, 2458.

3 Sahoo, D. P.; Patnaik, S.; Parida, K., Construction of a Z-Scheme Dictated WO_{3-x}/Ag/ZnCr LDH Synergistically Visible Light-Induced Photocatalyst Towards Tetracycline Degradation and H_2 Evolution. *ACS Omega* **2019**, *4*, 14721-14741.

4 Li, S.; Wang, L.; Li, Y.; Zhang, L.; Wang, A.; Xiao, N.; Gao, Y.; Li, N.; Song, W.; Ge, L.; Liu, J., Novel Photocatalyst Incorporating Ni-Co Layered Double Hydroxides with P-Doped Cds for Enhancing Photocatalytic Activity Towards Hydrogen Evolution. *Appl. Catal., B* **2019**, *254*, 145-155.

5 Zhang, G. H.; Lin, B. Z.; Yang, W. W.; Jiang, S. F.; Yao, Q. R.; Chen, Y. L.; Gao, B. F., Highly Efficient Photocatalytic Hydrogen Generation by Incorporating CdS into ZnCr-Layered Double Hydroxide Interlayer. *RSC Adv.* **2015**, *5*, 5823-5829.

6 Chen, J.; Wang, C.; Zhang, Y.; Guo, Z.; Luo, Y.; Mao, C.-J., Engineering Ultrafine NiS Cocatalysts as Active Sites to Boost Photocatalytic Hydrogen Production of MgAl Layered Double Hydroxide. *Appl. Surf. Sci.* **2020**, *506*, 144999.

7 Nayak, S.; Mohapatra, L.; Parida, K., Visible Light-Driven Novel g-C_3N_4/NiFe-LDH Composite Photocatalyst with Enhanced Photocatalytic Activity Towards Water Oxidation and Reduction Reaction. *J. Mater. Chem. A* **2015**, *3*, 18622-18635.

8 Zhou, H.; Song, Y.; Liu, Y.; Li, H.; Li, W.; Chang, Z., Fabrication of CdS/Ni-Fe LDH Heterostructure for Improved Photocatalytic Hydrogen Evolution from Aqueous Methanol Solution. *Int. J. Hydrogen Energy* **2018**, *43*, 14328-14336.

9 Zhou, P.; Liu, Y. Y.; Wang, Z. Y.; Wang, P.; Qin, X. Y.; Zhang, X. Y.; Huang, B. B.; Dai, Y., Efficient Photocatalytic Hydrogen Generation from Water over CdS Nanoparticles Confined Within an Alumina Matrix. *ChemPhotoChem* **2017**, *1*, 518-523.

10 Boppella, R.; Choi, C. H.; Moon, J.; Ha Kim, D., Spatial Charge Separation on Strongly

Coupled 2D-Hybrid of rGO/$La_2Ti_2O_7$/NiFe-LDH Heterostructures for Highly Efficient Noble Metal Free Photocatalytic Hydrogen Generation. *Appl. Catal., B* **2018**, *239*, 178-186.

11 Yao, L. H.; Wei, D.; Yan, D. P.; Hu, C. W., ZnCr Layered Double Hydroxide (LDH) Nanosheets Assisted Formation of Hierarchical Flower-Like CdZnS@LDH Microstructures with Improved Visible-Light-Driven H_2 Production. *Chem. Asian. J.* **2015**, *10*, 630-636.